Neuron, Vol. 32, 1041–1056, December 20, 2001, Copyright ©2001 by Cell Press

The Receptor Tyrosine Kinase EphB2 Regulates NMDA-Dependent Synaptic Function

Jeffrey T. Henderson,[1,4] John Georgiou,[1] Zhenping Jia,[2] Jennifer Robertson,[1] Sabine Elowe,[1,3] John C. Roder,[1] and Tony Pawson[1,3]

[1]Program in Molecular Biology and Cancer
Samuel Lunenfeld Research Institute
Mount Sinai Hospital
600 University Avenue
Toronto, Ontario M5G 1X5
Canada

[2]Department of Physiology

[3]Department of Molecular and Medical Genetics
University of Toronto
Toronto, Ontario M5S 1A8
Canada

Summary

Members of the Eph family of receptor tyrosine kinases control many aspects of cellular interactions during development, including axon guidance. Here, we demonstrate that EphB2 also regulates postnatal synaptic function in the mammalian CNS. Mice lacking the EphB2 intracellular kinase domain showed wild-type levels of LTP, whereas mice lacking the entire EphB2 receptor had reduced LTP at hippocampal CA1 and dentate gyrus synapses. Synaptic NMDA-mediated current was reduced in dentate granule neurons in *EphB2* null mice, as was synaptically localized NR1 as revealed by immunogold localization. Finally, we show that EphB2 is upregulated in hippocampal pyramidal neurons in vitro and in vivo by stimuli known to induce changes in synaptic structure. Together, these data demonstrate that EphB2 plays an important role in regulating synaptic function.

Introduction

EphB2 belongs to a large family of receptor tyrosine kinases (RTKs), which are involved in the cell-cell interactions required to organize complex tissues (Flanagan and Vanderhaeghen, 1998; Wang et al., 1999). Mammalian Eph receptors participate in boundary formation, cell adhesion, migration of the neural crest, and axon guidance (Drescher, 1997; O'Leary and Wilkinson, 1999). In addition, Eph RTKs regulate the topographic guidance of diverse groups of axons within the developing CNS and PNS (Birgbauer et al., 2000; Brownlee et al., 2000), as well as controlling aspects of axonal maturation (pruning) during this period (Brownlee et al., 2000; Gao et al., 1999). Furthermore, Eph receptors can regulate proper axonal crossing of the sagittal midline, as well as dorsoventral axon migration (Henkemeyer et al., 1996; Bergemann et al., 1998; Birgbauer et al., 2000).

Eph receptors are activated upon binding to ephrin ligands, which are themselves normally anchored to the cell surface (Holland et al., 1996). A-type ephrins, which activate EphA receptors, attach to the membrane through a glycosylphosphatidylinositol (GPI) group, while the B-type ephrins have a transmembrane region and bind EphB receptors (Flanagan and Vanderhaeghen, 1998; Gale et al., 1996). Eph receptor activation commonly results in reorganization of the cytoskeleton and cell repulsion (Bruckner and Klein, 1998; Meima et al., 1997; Elowe et al., 2001). Interaction of EphB2 receptors with cells expressing ephrinB ligands results not only in EphB2 activation, but also in the phosphorylation of tyrosines in the ephrinB cytodomain (Binns et al., 2000; Davis et al., 1994; Holland et al., 1996; Xu et al., 1999). Such data have suggested that ephrinB/EphB2 signaling may not be limited to activation of Eph RTK activity. Indeed, a mutant allele of murine EphB2 in which the kinase domain is replaced with β-galactosidase can support formation of the pars posterior of the anterior commissure, which is impaired in *EphB2* null mutants (Henkemeyer et al., 1996). Similarly, the *C. elegans* VAB-1 receptor exhibits both kinase-dependent and -independent functions (Chin-Sang et al., 1999; Wang et al., 1999).

A number of Eph receptors and their ligands continue to be expressed following the period of primary CNS innervation (i.e., Carpenter et al., 1995; Matsunaga et al., 2000), and Eph receptors can be localized to postsynaptic densities in the hippocampus (Buchert et al., 1999; Dalva et al., 2000; Torres et al., 1998). In addition, EphB2 interacts with the NMDA receptor NR1 subunit (NMDAR1) in cultured embryonic hippocampal neurons (Dalva et al., 2000; Grunwald et al., 2001). Association between EphB2 and NMDAR1 requires ephrin-induced EphB2 oligomerization but not EphB2 kinase activity, suggesting that this interaction is mediated through the extracellular domain of EphB2. These data raise the possibility that EphB2 plays a physiologic role in synaptic function.

Synaptic function in the brain requires the appropriate signaling and structural responses of a wide array of intracellular and membrane bound proteins. With respect to hippocampal LTP, NMDA-dependent signaling has been shown to play a central role, although postsynaptic AMPA, kainate, and metabotropic glutamate receptors, as well as additional presynaptic and postsynaptic proteins, have also been implicated in this process (Bortolotto et al., 1999; Gomperts et al., 2000; Malinow et al., 2000; Shi et al., 1999; Tang et al., 1999). While many of the molecular mechanisms regulating the induction and/or maintenance of LTP remain unclear, calcium and protein kinase second messengers, which interact with NMDARs, are known to be critical mediators of this process (Lisman et al., 1997; Sans et al., 2000; Soderling and Derkach, 2000).

We demonstrate here that the regional and cellular pattern of EphB2 expression changes markedly during the early postnatal period, in a manner that correlates with dendritic maturation and the upregulation of a number of genes known to be critical for synaptic function. In addition, we show that EphB2 expression is regulated

[4]Correspondence: henderson@mshri.on.ca

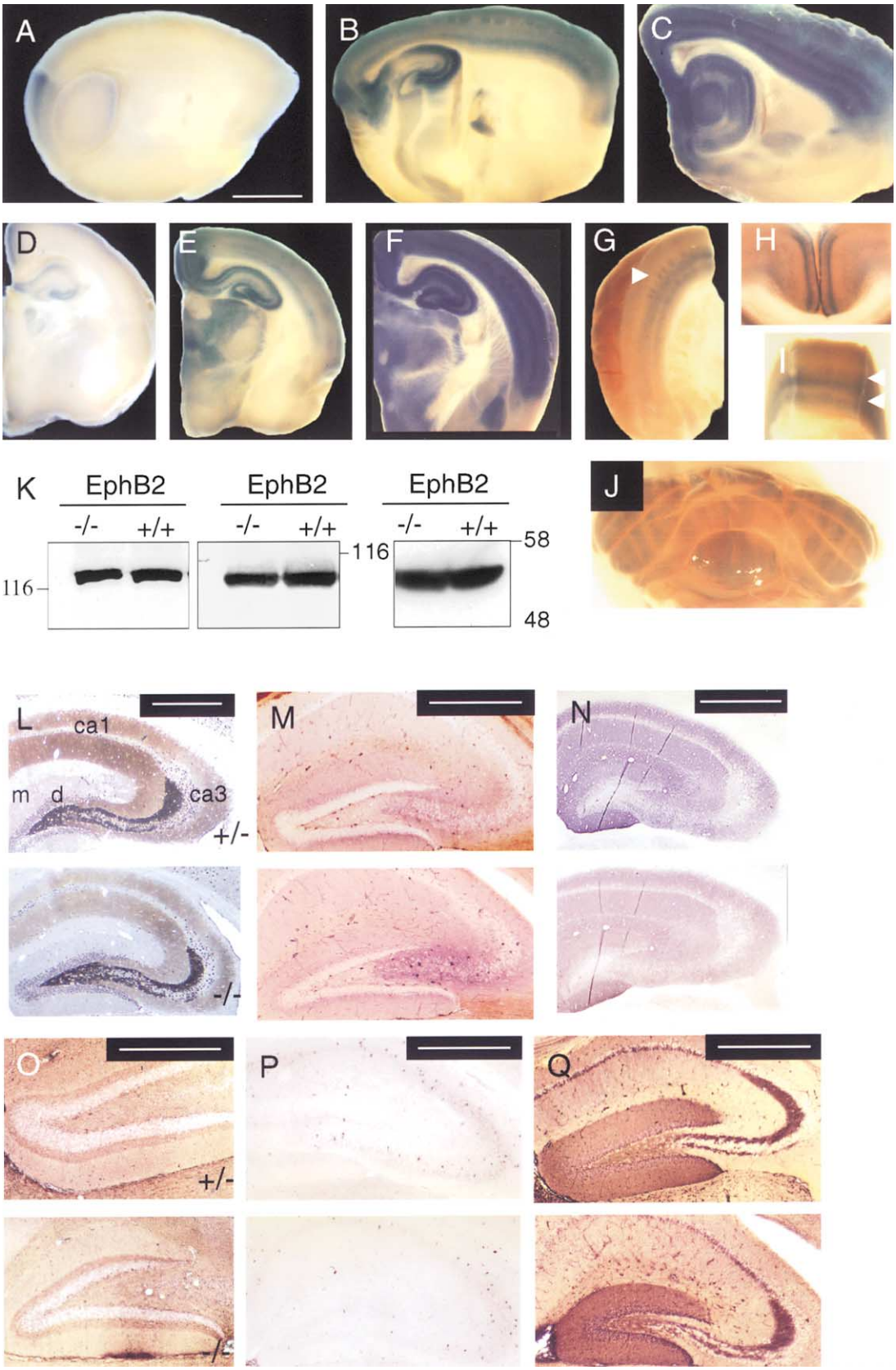

Figure 1. Expression of EphB2 and Hippocampal Markers during Postnatal Development

(A–J) Pattern of EphB2 during postnatal development as shown by Lac-Z staining in *EphB2*$^{+/N2}$ mice. (A and D) postnatal day (P)7, (B and E) P10, and (C and F) P35. Note the change in EphB2 expression between P7 and P10.

in an activity-dependent manner by stimuli known to induce synaptic plasticity. Finally, we demonstrate that *EphB2* null mice exhibit an attenuation of NMDA-dependent LTP at both Schaffer collateral/CA1 and perforant/dentate granule synapses, while *EphB2* mutants that lack kinase activity exhibit wild-type levels of LTP.

Results

EphB2 Expression Changes Markedly in the Early Postnatal Period

To examine EphB2 function in the postnatal CNS, we used mice heterozygous for a mutation of the *EphB2* gene (+/N2) in which the extracellular and juxtamembrane regions are fused to β-galactosidase (Henkemeyer et al., 1996). These animals, as well as homozygous N2/N2 mice, are neuroanatomically and functionally normal at all loci examined, including projections such as the pars posterior of the anterior commissure, which is defective in *EphB2* nulls (Henkemeyer et al., 1996). Similarly, $EphB2^{-/N2}$ mice are also neuroanatomically normal, indicating that a single *EphB2* N2 allele rescues the defects observed in *EphB2* nulls. Thus $EphB2^{+/N2}$ mice can be used to examine the wild-type pattern of EphB2 in the CNS. EphB2 expression changes markedly during the early postnatal period, coincident with postnatal synaptogenesis (Figures 1A–1J). While EphB2 is expressed in the brain during development, this expression is extinguished during late embryogenesis with the exception of the superior colliculus and ventral forebrain. However, by postnatal day (P)7, EphB2 is reexpressed at low levels within the hippocampus (predominantly CA3 and dentate gyrus) and medial entorhinal and cingulate corticies. By P10, the level and extent of EphB2 expression is increased, most prominently within the hippocampus and neocortex, as well as Purkinje dendrites, amygdala, geniculate, and thalamic and hypothalamic nuclei (Figures 1B and 1E), and continues into the adult period (Figures 1C and 1F–1J). In addition, by P10, EphB2 is expressed in a dorsoventral gradient throughout the neocortex and exhibits a laminated pattern of expression, which is higher in layers IV and VI (Figure 1I, arrowheads) and somatosensory barrels (Figure 1G, arrowhead). EphB2 also becomes expressed in a rostro-caudal pattern of stripes within Purkinje dendrites, similar to (but distinct from) that previously described for zebrin (Figure 1J).

Not only does the general pattern of EphB2 expression change during postnatal development, but the intracellular distribution of EphB2 changes as well during this period in neurons. The dominant embryonic pattern of EphB2 is one of high-axonal/low-dendritic expression during and immediately following target innervation (embryonic day [E]10–16). Postnatally, this pattern reverses, with EphB2 becoming expressed primarily in neuronal dendrites. As shown in Figures 1C and 1E–1G, EphB2 is absent in virtually all postnatal axonal tracts, a notable exception being hippocampal pyramidal neurons, which exhibit both axonal and dendritic EphB2 expression (see Figure 5A). The changes observed in EphB2 expression correlate with the pattern of dendritic maturation which occurs in the postnatal CNS and suggested to us that EphB2 may be involved in regulating postnatal synaptic function.

Loss of EphB2 Does Not Alter the Fundamental Circuitry or Fine Structure of the Hippocampus

To determine if EphB2 ablation altered the neuroanatomy of *EphB2* null hippocampi, several immunologic and ultrastructural assays were employed. Western analysis of NMDAR1 and GluR1 showed no quantitative difference between *EphB2* null mice and controls in hippocampal lysates (Figure 1K, left and middle panels, respectively). Timm's staining also showed a normal pattern of axonal and dendritic development for *EphB2* null pyramidal neurons, as well as a proper mossy fiber innervation (Figure 1L). Serial sections from *EphB2* null and control littermates also showed similar patterns of hippocampal staining for NADPH diaphorase (Figure 1M), GluR1 (Figure 1N), calretinin (Figure 1O), parvalbumin (Figure 1P), and calbindin (Figure 1Q). The unaltered pattern of the latter three proteins is significant, as developmental disturbances in neuronal architecture often disrupt the patterns of late born interneurons that express these markers.

To examine the hippocampal ultrastructure of *EphB2* null mice, CA1 and dentate granule neurons were examined via Golgi staining, electron microscopy (EM), and in retrogradely labeled fluorescent preparations. The morphology of CA1 dendrites in control (Figures 2A and 2C) and *EphB2* null (Figures 2B and 2D) mice did not differ significantly. Analysis of 75 μm segments of apical CA1 dendrite within the stratum radiatum of *EphB2* nulls and controls ($n \geq 9$ segments analyzed for each of four individuals per genotype) showed similar spine densities (102 ± 10 versus 118 ± 9 per 100 μm, respectively). The thickness of these dendritic shafts in *EphB2* nulls appeared greater than that of controls in both Golgi (Figure 2D versus Figure 2C) and fluorescent preparations (Figure 2F versus Figure 2E). However, analysis via EM cross-sections did not reveal significant differences in either CA1 or dentate neurons ($n \geq 22$ per genotype). Similarly, no significant differences in number (density), morphologic appearance, or class of pre-

(A–C) Interior parasagittal views of the cerebrum (orientation: left = caudal, right = rostral).
(D–F) Coronal sections at the level of the hippocampus (orientation: left = midline, right = distal).
(G–J) Added views of EphB2 expression at P35. (G) EphB2 staining at the level of the PBSF (arrowhead), (H) cingulate, (I) EphB2 staining in cortical layers; EphB2 is particularly prominent in layers IV and VI (arrowheads), and (J) cerebellum.
(A–J) Scale bar (A) represents 3 mm.
(K) Whole hippocampal lysates from P35 $EphB2^{-/-}$ and $EphB2^{+/+}$ mice probed for NMDAR1 (left), GluR1 (middle), and α-tubulin (right).
(L–Q) Staining pattern of hippocampal markers in adult $EphB2^{+/-}$ (top) and $EphB2^{-/-}$ (bottom) mice. (L) Timm's, (M) NADPH diaphorase, (N) GluR1, (O) calretinin, (P) parvalbumin, and (Q) calbindin. Scale bars equal 500 μm for (L) and (P–Q); 1 mm for (M) and (N). Photomicrographs are oriented as indicated in (L) with the sagittal midline (m) to the left, dentate (d) subregion.

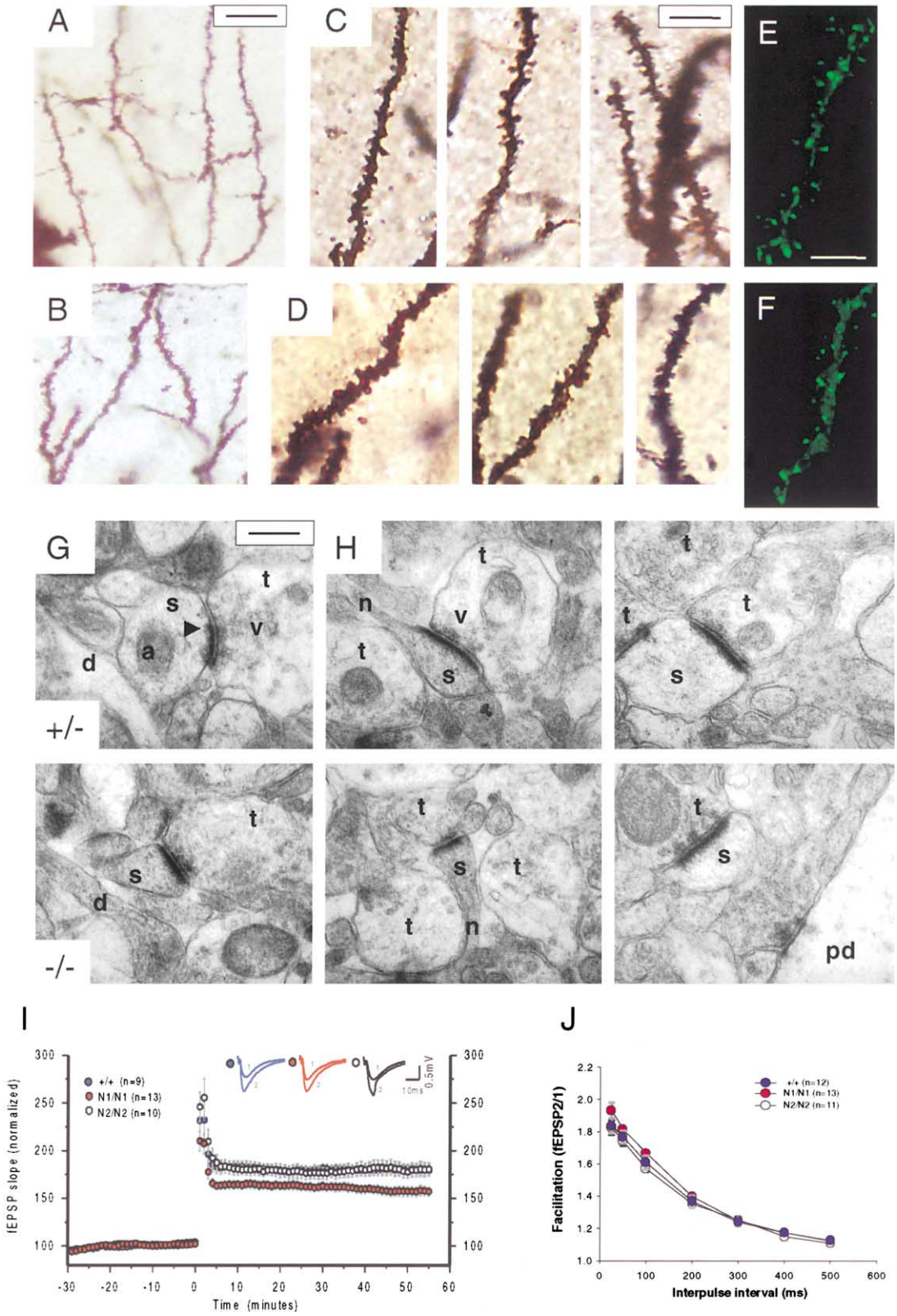

Figure 2. Ultrastructure and Attenuation of LTP in Schaffer Collateral/CA1 Synapses of *EphB2* Null Mice

(A–D) Golgi impregnated apical dendrites of CA1 neurons in vivo in *EphB2*$^{+/-}$ (A and C) and *EphB2*$^{-/-}$ (B and D) mice. Sections are oriented so that the distal portions of the dendrite extends toward the top of the photomicrograph. Scale bar equals 20 μm in (A) and (B), and 8 μm for (C) and (D).

(E and F) Fluorescent images of FITC-dextran labeled CA1 dendrites showing synaptic spines in *EphB2*$^{+/-}$ (E), and *EphB2*$^{-/-}$ (F) mice, respectively. Scale bar, 10 μm.

synaptic or postsynaptic terminals were observed in *EphB2* null mice versus controls by EM at either CA1 (Figure 2G) or the dentate gyrus (Figure 2H). This lack of neuroanatomic perturbation is, perhaps, not surprising given the absence of EphB2 expression in these structures during embryonic and neonatal development.

EphB2 Null Mice Exhibit a Reduction in LTP

Despite the absence of neuroanatomical defects, *EphB2* null mice exhibited a significant attenuation in LTP. As shown in Figure 2I, field recordings of Schaffer collateral/CA1 responses in *EphB2* null mice show a significant reduction in LTP compared to wild-type littermates (157.6% ± 4.6%, n = 13 versus 180.4% ± 5.3%, n = 9; p = 0.004). However, mice homozygous for the *EphB2* N2 allele exhibited wild-type levels of LTP (180.2% ± 7.3%, n = 10; p = 0.98), demonstrating that the reduction in LTP is independent of EphB2 kinase activity (Figure 2I). Examination of paired pulse facilitation in CA1 (Figure 2J) demonstrated no differences between $EphB2^{-/-}$ mice and controls, suggesting that the defect in LTP was not due to presynaptic effects.

To pursue the role of EphB2 in hippocampal function, we examined the induction of LTP in perforant path/dentate granule synapses. As in CA1, NMDARs mediate a substantial component of LTP at this site, and EphB2 is strongly expressed in dentate granule dendrites. However, in contrast to axons of CA1 pyramidal neurons, dentate mossy fibers do not express EphB2 nor do their innervating perforant path fibers. Thus, dentate synapses provide a more defined system to test EphB2 function. Examination of dentate granule responses in slices from $EphB2^{+/+}$, $EphB2^{+/-}$, and $EphB2^{-/-}$ mice revealed reductions in posttetanic potentiation and LTP (Figure 3) for *EphB2* null mice which were of greater magnitude than that observed for CA1. The average fEPSP slopes within the first 2 min after the tetanus (4 trains, 100 Hz/0.5 s, 20 s apart), was 318% ± 21% in wild-type mice $EphB2^{+/+}$ (8 slices/4 mice) and 210% ± 19% in *EphB2* nulls (−/−) (10 slices/5 mice); this difference is significant (p = 0.002, t test). Animals heterozygous for $EphB2^{+/-}$ exhibited intermediate levels of LTP (271% ± 10%, 13 slices/7 mice; p = 0.02 compared to wild-type). When compared 90 min after tetanus, LTP in $EphB2^{-/-}$ slices was severely affected compared to wild-type controls (116% ± 9% versus 173% ± 12%, respectively, p = 0.001). For $EphB2^{+/-}$ mice, this value was 156 ± 7% at 90 min posttetanus (p = 0.002 in comparison to *EphB2* nulls, p = 0.22 in comparison to [+/+] littermates). Similar to CA1, $EphB2^{N2/N2}$ mice exhibited normal levels of LTP (Figure 3B). Thus, loss of EphB2 largely abolishes the sustained, late phase of LTP, and these effects are independent of *EphB2* kinase activity.

Following induction of LTP, further tetanic stimulation normally produces additional elevations in synaptic responses. In contrast to control littermates, successive trains of stimulation were not effective in potentiating synaptic responses in *EphB2* null mice (Figure 3C, closed triangles). Thus, successive trains of high frequency stimulation cannot compensate for the loss of EphB2.

Altered presynaptic and/or postsynaptic properties, as well as inhibitory tone may contribute to the defects in synaptic plasticity observed in $EphB2^{-/-}$ mice. The efficiency of synaptic coupling between presynaptic and postsynaptic neurons, as depicted by the input-output relationship (fEPSP versus stimulus intensity), was unaffected in $EphB2^{-/-}$ mice (Figure 3D, left; p > 0.25). Moreover, the contribution of inhibitory neurons to synaptic response appears unchanged in *EphB2* null mice, given that the input-output relationship was enhanced to the same extent in $EphB2^{+/+}$, $EphB2^{+/-}$, and $EphB2^{-/-}$ mice after the addition of picrotoxin to block $GABA_A$-mediated influences (Figure 3D, right; p > 0.11). Thus, differences in baseline stimulation cannot account for the LTP deficiencies observed in *EphB2* null mice. Presynaptic modulation of synaptic transmission (Wang and Wojtowicz, 1997) was also unaffected in *EphB2* null mice. Paired-pulses delivered 10–600 ms apart also elicited similar levels of depression in $EphB2^{-/-}$, $EphB2^{+/-}$, and $EphB2^{+/+}$ slices (Figure 3E). Data in Figures 3D and 3E represent repetitions of four, seven, and five for $EphB2^{+/+}$, $EphB2^{+/-}$, and $EphB2^{-/-}$ mice, respectively. Basal synaptic responses between wild-type and $EphB2^{-/-}$ fEPSPs for experiments shown in Figure 3A were also not significantly different (−0.52 ± 0.02 mV/ms versus −0.56 ± 0.04 mV/ms, respectively, p = 0.36). Thus, we observe no impairments in presynaptic function and/or synaptic coupling for dentate granule cells. These data suggest that the observed LTP deficits are mediated by postsynaptically localized EphB2 receptors.

Synaptic NMDA Currents Are Reduced in Mice Lacking EphB2

The LTP deficit in $EphB2^{-/-}$ mice may reflect functional changes in NMDARs. We therefore directly examined NMDAR function by measuring its contribution to evoked glutamatergic synaptic current. Granule neurons were clamped at holding potentials between −80 and +60 mV, and synaptic currents were evoked by stimulation of the medial perforant path. Synaptic currents of $EphB2^{+/+}$ and $EphB2^{-/-}$ mice were similar (Figure 3F). Addition of the NMDAR blocker D-AP5 reduced EPSCs, especially at positive cell holding potentials (Figure 3F, traces labeled as +AP5). Subsequent addition of NBQX to block AMPA receptors eliminated more than 80% of

(G and H) Electron photomicrographs of CA1 (G), and dentate synapses (H) from $EphB2^{+/-}$ and $EphB2^{-/-}$ mice as indicated in figure. Scale bar equals 0.3 μm (s = dendritic spine, t = nerve terminal/bouton, a = spine apparatus, v = presynaptic vesicles, n = spine shaft/neck, d = dendrite, and pd = primary dendrite with associated axo-dendritic synapse).

(I) Analysis of LTP in wild-type, $EphB2^{-/-}$, and $EphB2^{N2/N2}$ mice. Plotted are representative traces (average of four sweeps) of fEPSPs obtained immediately before (1) and 50 min after (2) tetanic stimulation.

(J) Analysis of paired pulse facilitation in CA1 synapses for $EphB2^{+/+}$ and $EphB2^{-/-}$ mice. Plot denotes the degree of facilitation in the second fEPSP slope of trace (2) compared with trace (1) (see inset in [I]) as a function of interpulse interval.

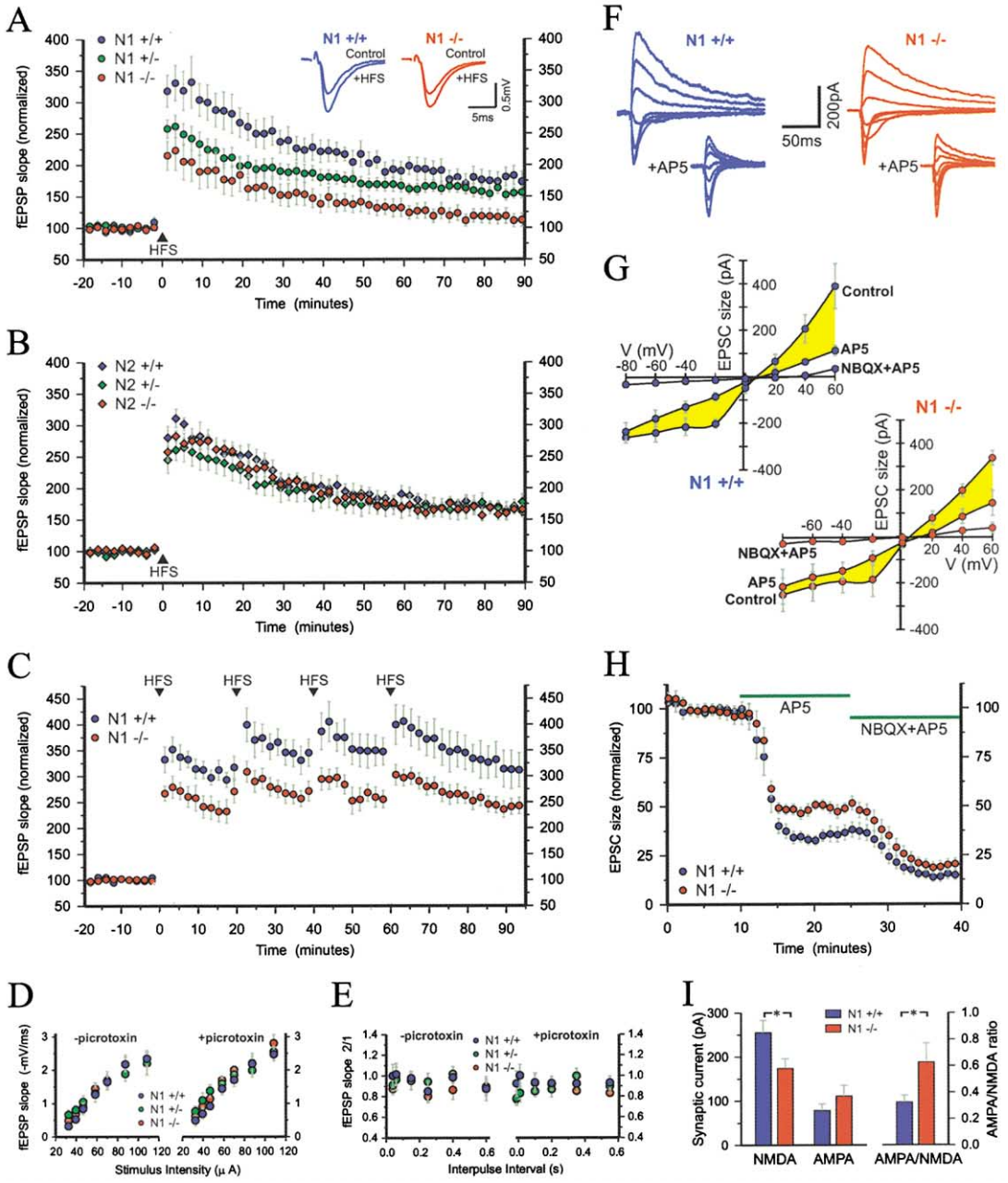

Figure 3. Reduction of LTP in Dentate Gyrus of *EphB2* Null Mice

(A) Analysis of LTP in perforant/dentate granule synapses of *EphB2*$^{+/+}$ (8 slices/4 mice), *EphB2*$^{+/-}$ (13 slices/7 mice), and *EphB2*$^{-/-}$ (10 slices/5 mice) mice. High frequency stimulation (HFS) was delivered via medial perforant path at t = 0 (closed triangle). Insert shows representative fEPSPs (average of six) before and after tetanus for *EphB2*$^{+/+}$ (blue) and *EphB2*$^{-/-}$ (red) mice.

(B) LTP in dentate synapses of *EphB2*$^{+/N2}$ mice (6 slices/3 mice/genotype).

(C) Saturation of LTP in *EphB2*$^{+/+}$ and *EphB2*$^{-/-}$ mice (7 slices/6 wild-type mice and 9 slices/6 null mice). HFS was applied four times as indicated (closed triangle).

(D) Input/output relationship within dentate synapses in the absence (left) and presence (right) of picrotoxin for *EphB2*$^{+/+}$; 4 slices/4 mice, *EphB2*$^{+/-}$; 7 slices/7 mice, and *EphB2*$^{-/-}$; 5 slices/5 mice.

(E) Paired pulse depression within the dentate gyrus in the absence (left) and presence (right) of picrotoxin from same slices as in (D).

(F) Whole-cell recordings of EPSCs from single dentate granule neurons in response to medial perforant path stimulation of wild-type *EphB2*$^{+/+}$ (blue traces) and null *EphB2*$^{-/-}$ (red traces) mice (holding potentials between –80 and +60 mV). Control EPSCs appear on the top and currents obtained after NMDA blocker D-AP5 addition appear below (+AP5).

(G) Current voltage relationship in dentate granule cells from *EphB2*$^{+/+}$ (blue traces, 4 cells/slices from three mice) and null *EphB2*$^{-/-}$ mice (red traces, 4 cells/slices from four mice). NMDA currents were removed pharmacologically by addition of AP5, and AMPA receptors were subsequently blocked by further addition of NBQX. Difference between control and AP5 curves (shaded in yellow) represents the NMDA current.

(H) Normalized synaptic currents from neurons held at +60 mV and sequentially exposed continuously to the indicated blockers (green bars). Number of repetitions for *EphB2*$^{+/+}$ and *EphB2*$^{-/-}$ was 11 cells/slices from five mice and 10 cells/slices from five mice, respectively.

(I) NMDA and AMPA current, as well as the AMPA/NMDA ratio, was calculated from EPSCs obtained in experiments shown in (H).

Table 1. Analysis of NMDAR1 Immunogold Labeling within the Dentate

Structure	*EphB2* genotype (N1) (+/−)	(−/−)
Postsynaptic density:		
Particles/synapse	2.61 ± 0.19	1.52 ± 0.13*
Particles/μm^2 within PSD zone	229 ± 38	139 ± 29*
Particles/PSD (absolute range)	0 − 9	0 − 5
Total particle count	601	345
Average PSD length (μm)	0.457 ± 0.059	0.438 ± 0.068
Synapses analyzed per animal	120, 110	120, 110
Dendritic cytoplasm:		
Particles/μm^2	44.5 ± 6.22	57.4 ± 7.18
Number of structures analyzed per animal	60, 60	60, 60
Dentate nuclei, particles/μm^2	3.21 ± 0.43	3.60 ± 0.57
Nuclei examined per animal	10, 10	10, 10
Formvar coating, particles/μm^2	0.22 ± 0.04	0.24 ± 0.02

Postsynaptic density counts reflect numbers of immunogold particles associated with synaptic membrane.
Dendritic cytoplasm refers to dendritic immunogold labeling not associated with dendritic plasma membrane or spinous processes.
Data shown ± SE.
Asterisk denotes statistical significance at $p < 0.05$.

EPSC (Figure 3G, "NBQX + AP5"). These data indicate that NMDA and AMPA receptors mediate the majority of evoked synaptic responses in *EphB2*$^{+/+}$ and *EphB2*$^{-/-}$ granule cells. The current voltage (I/V) relationships under these experimental conditions are shown in Figure 3G (4 cells/slices from three wild-type mice and 4 cells/slices from four *EphB2* null mice). The NMDA current component (difference between control and AP5 plots, shaded portions Figure 3G) was reduced in *EphB2* nulls compared to controls. We further quantified this difference in NMDA current, by sequentially perfusing slices with D-AP5 and the AMPA receptor blocker NBQX (Figure 3H). Dentate granule neurons were held at +60 mV, a holding potential where synaptic current is carried largely by NMDARs. The average amplitude of the initial control EPSC was 388 ± 40 and 350 ± 47 pA for neurons from *EphB2*$^{+/+}$ and *EphB2*$^{-/-}$ mice, respectively (11 cells/slices from five wild-type mice and 10 cells/slices from five null mice); the difference in control current between these genotypes was not significant ($p = 0.55$). To derive the NMDA current, we determined the reduction in EPSC size, which occurred after addition of AP5, and this represented 174 ± 21 and 255 ± 28 pA in neurons from EphB2$^{-/-}$ and *EphB2*$^{+/+}$ mice, respectively (Figure 3I). Thus, NMDA-mediated current was significantly reduced in neurons from *EphB2*$^{-/-}$ mice compared to controls ($p = 0.03$). The AMPA contribution was subsequently revealed by determining the reduc-

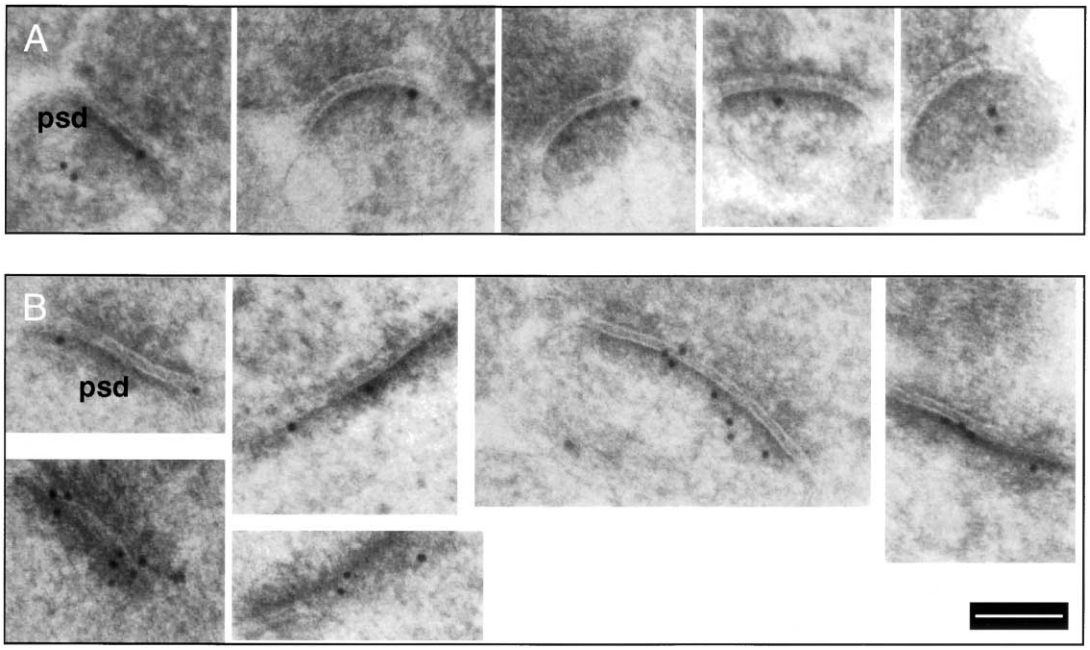

Figure 4. Immunogold Labeling of NMDAR1 at Axo-Dendritic Granule Synapses within the Dentate Molecular Layer
(A) Examples of synaptic labeling for 5-week-old *EphB2*$^{-/-}$ (A) and *EphB2*$^{+/-}$ (B) mice. Scale bars equal 100 nm.

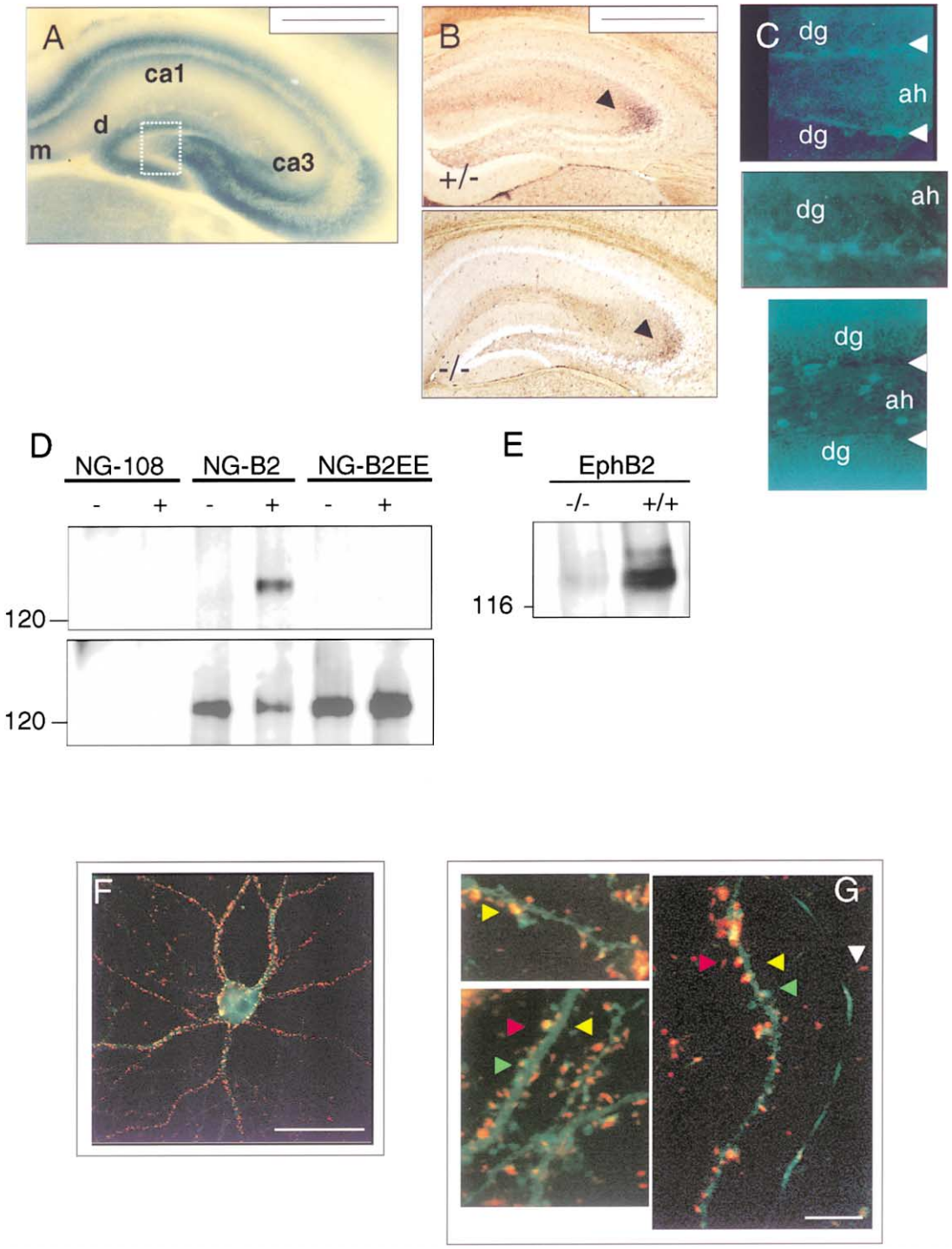

Figure 5. Localization of EphB2 and Ephrin Expression In Vivo and In Vitro

(A) Pattern of EphB2 expression in adult hippocampus as shown by β-galactosidase staining in *EphB2*$^{+/N2}$ mouse. CA1, CA3, dentate (d), and orientation toward the midline (m) are indicated. Dotted square denotes region shown in Figure 4C. Scale bar, 1 mm.

(B) Staining for ephrin B1 in hippocampus. Note staining in mossy fibers (arrowhead).

(C) Top and middle panels show localization of phosphorylated EphB (arrowheads) proximal to inner dentate granule cell layer (dg) by immunofluorescence. Bottom panel shows adjacent section stained for GluR1 to aid in orientation of dentate structures (ah = axon hilus).

(D) 435J antibody specifically recognizes phosphorylation at tyrosines Y_{604} and Y_{610} within the EphB2 juxtamembrane region. Control (−) and ephrin B1 challenged (+, 2 μg/ml) NG-108, NG-108/EphB2 transfected (NG-EphB2), and NG-108/EphB2 transfected Y/E_{604}, Y/E_{610} mutant (EphB2EE) cells were lysed in PLC buffer and immunoprecipitated with anti-EphB2. Samples were resolved by SDS-PAGE, and immunoblotted with 435J antibody (upper panel). The blot was reprobed with anti-EphB2 (lower panel).

(E) To determine levels of activated EphB2 expression in the adult hippocampus, hippocampal lysates from *EphB2*$^{-/-}$ and *EphB2*$^{+/+}$ mice were immunoprecipitated with anti-EphB2 and immunoblotted with 435J. Equivalence of loading was verified by blotting with α-tubulin as in Figure 1K.

tion in EPSC size that occurred after switching to ACSF containing AP5 and NBQX. The synaptic current mediated by AMPA in EphB2$^{+/+}$ and *EphB2*$^{-/-}$ slices was not significantly different (78 $\pm$ 14 versus 111 $\pm$ 25 pA, $p = 0.26$). The deficit in NMDA (but not AMPA) current in *EphB2* null neurons compared to controls resulted in an increased AMPA/NMDA ratio of glutamatergic synaptic current (Figure 3I) and directly indicates that NMDAR function is compromised in mice lacking EphB2.

Distribution of NMDAR1 in Dentate Granule Neurons

The data above demonstrate that *EphB2* null mice exhibit reductions in LTP at both Schaffer collateral CA1 and perforant path dentate synapses and exhibit a decrease in NMDA-dependent current. To gain insight into the basis of these effects, we examined the distribution of NMDAR1 in dentate granule neurons of *EphB2* null mice by immunogold labeling. Though dendritic spines of *EphB2*$^{-/-}$ dentate granule neurons exhibit a normal morphologic appearance (Figure 2H and Table 1), *EphB2* null mice demonstrate a 40% reduction in their level of NMDAR1 associated with the postsynaptic density (PSD) in asymmetric axo-spinous synapses (Figure 4 and Table 1). In addition, levels of NMDAR1 labeling within dentate dendrites not associated with the cell membrane exhibited a trend toward higher particle densities in *EphB2*$^{-/-}$ mice compared to controls, though this did not reach statistical significance (Table 1). These data indicate that loss of EphB2 reduces levels of PSD associated NMDAR1. Ablation of EphB2 appears to result in a redistribution of NMDAR1, rather than reducing total NMDAR1 levels, since we observed no overt differences in the cellular pattern of NMDAR1 staining for *EphB2*$^{-/-}$ and *EphB2*$^{+/+}$ dentate granule neurons in vivo (data not shown), and total hippocampal levels of NMDAR1 are similar between these two groups (Figure 1K). Whether the observed changes in NMDAR1 distribution reflect a change in membrane targeting or a reduction in the synaptic stability of this protein is as yet undetermined.

Eph/ephrin Expression in Hippocampal Neurons

To understand the regulation of Eph/ephrin interactions within the hippocampus, we examined dentate granule neurons in further detail. Figure 5A shows the pattern of EphB2 expression in the P10 adult hippocampus as measured by LacZ staining. In dentate granule neurons, EphB2 expression is dendritic and is not expressed in the polymorphic layer or mossy fiber termination zone (see also Figures 6D and 6F). In contrast, ephrin B1 is concentrated to mossy fiber terminals (Figure 5B), suggesting that Eph/ephrin expression is segregated to different compartments in these neurons. To determine the in vivo pattern of receptor activation within the dentate gyrus, we stained hippocampal sections with a phosphospecific antibody (435J) that specifically recognizes phosphorylation at Y_{604} and Y_{610} within the EphB2 juxtamembrane region, which occurs following ligand binding. Receptor phosphorylation is observed within the inferior aspect of the cellular layer of the dentate gyrus at the interface of EphB2/ephrin expression (Figure 5C). The 435J antibody is specific for phospho-EphB2, since it recognizes EphB2 in ephrin B1 stimulated NG-108 cells expressing the wild-type receptor (NG-EphB2), but not in unstimulated NG-EphB2 cells, nor in stimulated cells expressing an EphB2 mutant in which tyrosines 604 and 610 are mutated to glutamate (Figure 5D). To verify that EphB2 is phosphorylated at these tyrosines in the adult hippocampus, hippocampal lysates from *EphB2*$^{-/-}$ and *EphB2*$^{+/+}$ were immunoprecipitated with anti-EphB2 and immunoblotted with the 435J. EphB2 exhibits substantial phosphorylation under these conditions (Figure 5E).

To determine the distribution of activated EphB2 in hippocampal neurons, cultured pyramidal neurons (P0, cultured 5 weeks in vitro) were stained for 435J (green) and the presynaptic marker synaptophysin (red). Staining for 435J is observed in the dendritic shaft and spine as well as neural axons, similar to the pattern seen for these neurons in vivo (Figures 5F and 5G). Some dendritic spines exhibit juxtaposed staining of both synaptophysin and EphB2 (yellow arrowhead), while others exhibit EphB2 staining alone (green arrowhead). Thus, activated EphB2 is observed in only a subpopulation of pyramidal dendritic spines.

EphB2 Is Upregulated Following Glutaminergic Stimulation in the Hippocampus In Vivo

As shown above, EphB2 plays a role in regulating activity-dependent synapse function. To determine if stimulus input may reciprocally regulate EphB2 expression, we examined models of postnatal synaptic plasticity. Implantation of 1 nmol of kainic acid into adult hippocampi (Figure 6A) induced degeneration of pyramidal neurons (Figure 6B), in turn promoting the sprouting of mossy fiber collaterals. Kainic acid and saline-treated hippocampi were isolated from *EphB2*$^{+/+}$ mice 1 week following treatment. Western analysis of these hippocampal lysates demonstrate that both EphB2 and ephrin B1 were modestly upregulated (2-fold) following kainic acid treatment (Figure 6C). To more specifically determine the sites of EphB2 upregulation, expression was monitored using EphB2$^{+/N2}$ mice. As shown in Figures 6D–6F, EphB2 expression was strongly upregulated in dendrites of dentate granule neurons following kainic acid, but not saline treatment. This increase was strongest in the dendritic region proximal to the granule cell layer (Figure 6E). EphB2 expression did not rise immediately following kainic acid treatment, but rather increased gradually over several days and persisted for the longest time point examined (5 weeks, data not shown).

To determine if loss of EphB2 had functional conse-

(F) EphB2 (green)/synaptophysin (red) expression in hippocampal pyramidal neuron cultured for 5 weeks in vitro.
(G) Higher magnification view of EphB2/synaptophysin expression in pyramidal dendritic spines. Some dendritic spines exhibit both synaptophysin (red arrowhead) and EphB2 staining (yellow arrowhead), while others exhibit EphB2 staining alone (green arrowhead). Open arrowhead indicates EphB2 staining in hippocampal axon. For (F) and (G), scale bars equal 50 and 10 μm, respectively.

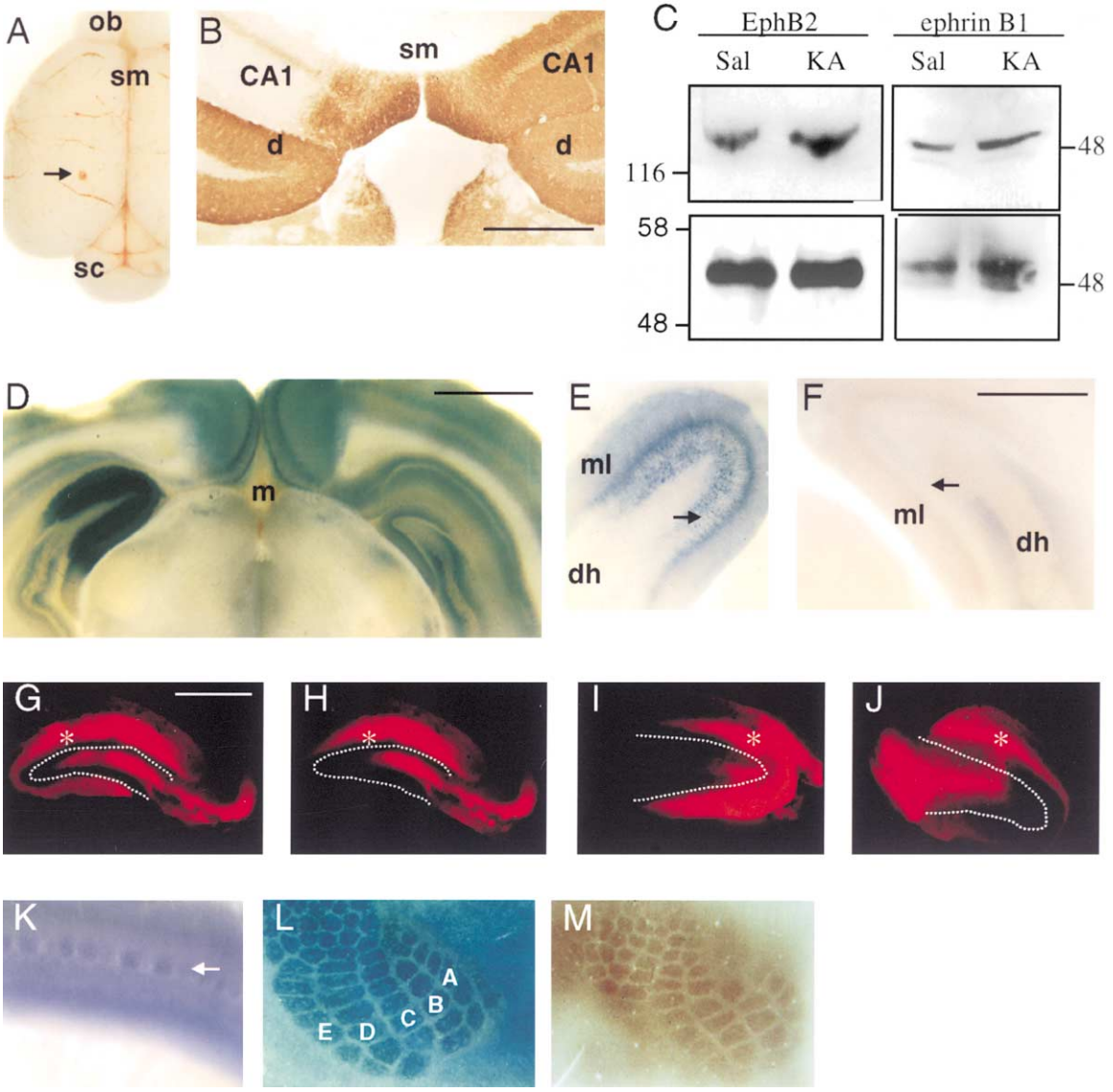

Figure 6. EphB2 Expression Following Kainic Acid Stimulation

(A) Overview showing location of cannula placement (arrow) for deposition of drugs into hippocampus (top = rostral, bottom = caudal, ob = ofactory bulb, sm = sagittal midline, and sc = superior colliculus).

(B) GluR1 staining in kainic acid (left) and saline (right) treated hippocampi of *EphB2*$^{+/N2}$ mouse 1 week following treatment. CA1, dentate gyrus (d), and sagittal midline (sm) are indicated. Scale bar, 0.5 mm.

(C) EphB2/ephrin expression in hippocampal lysates from saline (sal) and kainic acid (KA) treated hippocampi of *EphB2*$^{+/+}$ mice (opposing sides of same animal). Hippocampal lysate probed for EphB2 (top left) or ephrin B1 (top right). (Bottom right) ephrin B1 blot reprobed for phospho-tyrosine. (Bottom left) Reprobe for α-tubulin.

(D) Pattern of β-galactosidase staining in kainic acid (left) and saline (right) treated hippocampi of *EphB2*$^{+/N2}$ mouse 1 week following treatment. Scale bar, 1 mm.

(E and F) Higher magnification views of the dentate in kainic acid (E) and saline (F) treated hippocampi 5 days following treatment indicating location and intensity of EphB2 expression relative to molecular (ml) and dentate granule cell (arrow) layers (m = sagittal midline, dh = dentate hilus). A 10-fold greater development time was used to obtain the pattern shown in (D) compared to (E) and (F).

(G–J) DiI labeling of saline (G and H) and kainic acid (I and J) treated hippocampi 4 weeks following treatment in *EphB2*$^{+/-}$ (G and I) and *EphB2*$^{-/-}$ (H and J) mice. Samples were obtained at the same rostral-caudal level. Location of DiI placement is indicated by an asterisk, dentate granule layer by dotted line. Scale bar, 500 μm. For (G) and (H), sagittal midline is on the left; for (I) and (J), it is on the right.

(K) Coronal view of EphB2 expression as measured by β-galactosidase staining in somatosensory cortical barrels (arrow) in *EphB2*$^{+/N2}$ mouse at P35.

(L) Tangential view of EphB2 expression in PMBSF at P35.

(M) Cytochrome oxidase staining within PMBSF of *EphB2*$^{-/-}$ mouse at P35.

(L) and (M) represent composites of successive tangential sections.

quences with respect to kainic acid induced mossy fiber sprouting, *EphB2*$^{+/-}$ and *EphB2*$^{-/-}$ mice were sacrificed 4 weeks following stereotactic kainic acid implantation. As shown in Figure 6, mossy fiber sprouting was determined by DiI labeling in saline (Figures 6G and 6H) and kainic acid treated (Figures 6I and 6J) hippocampi from *EphB2*$^{+/-}$ (Figures 6G and 6I) and *EphB2*$^{-/-}$ (Figures 6H and 6J) mice, respectively. Both groups showed the expected pattern of dendritic and axonal labeling for saline-treated hippocampi (Figures 6G and 6H). However, while *EphB2*$^{+/-}$ and *EphB2*$^{+/+}$ mice showed the expected pattern of mossy fiber sprouting following kainic acid treatment with a loss of innervation to CA3, *EphB2* null mice exhibited a strong aberrant projection toward the dentate hilus (Figure 6J).

To determine if elevation of EphB2 expression is a general feature of synaptic plasticity, several additional models of plasticity were examined. EphB2 is expressed in cortical barrels postnatally in a pattern similar to the general synaptic marker cytochrome oxidase (Figures 6K and 6L). *EphB2*$^{+/N2}$ mice, which underwent whisker ablation at P0, showed no elevation in EphB2 expression within either cortical barrels or trigeminal barrelets (data not shown), despite expansion of adjacent cortical barrels into the ablated field. Furthermore, axotomy of facial motor or dorsal cutaneous axons at P10 and P30, respectively, did not result in an alteration of EphB2 expression in effected axons or cell soma, nor did monocular deprivation during the critical period (P22–P29) in ocular columns of the superior colliculus (data not shown). Thus, upregulation of EphB2 appears to occur only for specific forms of synaptic plasticity.

Regulation of EphB2 Expression at Hippocampal Neurons In Vitro

We explored the mechanism by which kainic acid enhances EphB2 expression in P7 hippocampal neurons in vitro. In the absence of added agents, dissociated hippocampal neurons exhibited a rapid (12–20 hr) loss of EphB2 expression (Figure 7A), despite good neuronal viability. The loss of EphB2 expression correlated with neuronal dissociation, as hippocampal (Figure 7B) or spinal cord (Figure 7C) explants maintained EphB2 expression for weeks under culture conditions. To determine if glutaminergic activity played a role in this process, hippocampal cultures were exposed to kainic acid and NMDA. These agents resulted in the maintenance of EphB2 expression in a subpopulation of pyramidal neurons (2%–5% of total) (Figures 7D and 7E). In these cultures, EphB2 tended to be expressed at cell-cell interfaces and was never observed in isolated neurons, even in the presence of NMDA. Kainic acid and NMDA may thus act in concert with factors such as ephrinB ligands, which are expressed in these neurons. Though kainic acid induces neurotrophins such as BDNF and NT-3 in the hippocampus in vivo (Lee et al., 1997; Rudge et al.,1998), treatment with NGF, NT-3, BDNF, GDNF, IL-6, and CNTF, either alone or in combination, failed to induce EphB2 in acutely dissociated pyramidal neurons (data not shown).

Finally, EphB2 expression was examined in *EphB2*$^{N2/+}$ hippocampal neurons plated at P7 and cultured for $>$14 days. During this period, neurons became reinnervated and EphB2 became reexpressed at points of synaptic contact (Figure 7F, closed and open arrowheads), whereas neurons which remained synaptically isolated did not express EphB2 (Figure 7G). Thus, glutaminergic stimuli and synaptic innervation positively regulate EphB2 expression in hippocampal neurons in vitro.

Discussion

Expression of EphB2 in the Postnatal CNS

Eph receptors have been shown to control the topographic guidance and maturation of specific axons during neural development. We demonstrate here that EphB2 also participates in the modification of synaptic function postnatally in regions associated with learning and memory. Consistent with this role, EphB2 is induced in CNS regions which undergo activity-dependent modification during synaptic maturation. Analysis of dentate granule and hippocampal pyramidal neurons in vivo and in vitro demonstrates that EphB2 is expressed in dendritic regions during this period, in contrast to its largely axonal distribution during embryogenesis (Henkemeyer et al., 1996). In dendrites, EphB2 is localized to both the shaft and spines in hippocampal neurons in vitro. Staining with phosphospecific anti-EphB2 antibodies demonstrates that activated EphB2 receptors are preferentially localized to subpopulations of pyramidal dendritic spines in vitro. Consistent with this, EphB2 has been localized to the synaptic membrane in rat cortex and colocalizes with synaptophysin in E17 hippocampal neurons cultured for 2 weeks in vitro (Dalva et al., 2000; Torres et al., 1998). Interestingly, EphB2 is more highly expressed in NMDAR rich regions, such as proximal components of dentate and pyramidal dendrites (Milner and Drake, 2001), suggesting that it may preferentially affect particular synaptic inputs, while ephrin B1 is strongly expressed in regions such as dentate mossy fibers. Thus, in dentate granule neurons, EphB2 and at least one of its ligands are expressed in specific intracellular regions.

Structural Organization of Hippocampus in *EphB2* Null Mice

While it is difficult to rule out subtle developmental alterations in hippocampal structure in *EphB2* null mice, several lines of evidence suggest that this does not occur. Morphologically, the major afferent inputs, efferent projections, and intrinsic neuroanatomy of the hippocampus are unperturbed in *EphB2* null mice. In addition, *EphB2* null mice show no differences in Timm's staining of mossy fibers or the expression of immunohistochemical markers indicative of hippocampal morphology. Similarly, CA1 dendritic ultrastructure and dentate granule morphology examined by Golgi staining, fluorescent tracing, and EM did not differ between *EphB2* null and control mice. Tests of basal synaptic transmission also revealed no differences between *EphB2*$^{-/-}$, *EphB2*$^{+/-}$, and *EphB2*$^{+/+}$ mice. This is, perhaps, not surprising since EphB2 is not expressed within the developing hippocampus or its targets from E14 to birth, with the possible exception of the ventral septum of the forebrain (Henkemeyer et al., 1996).

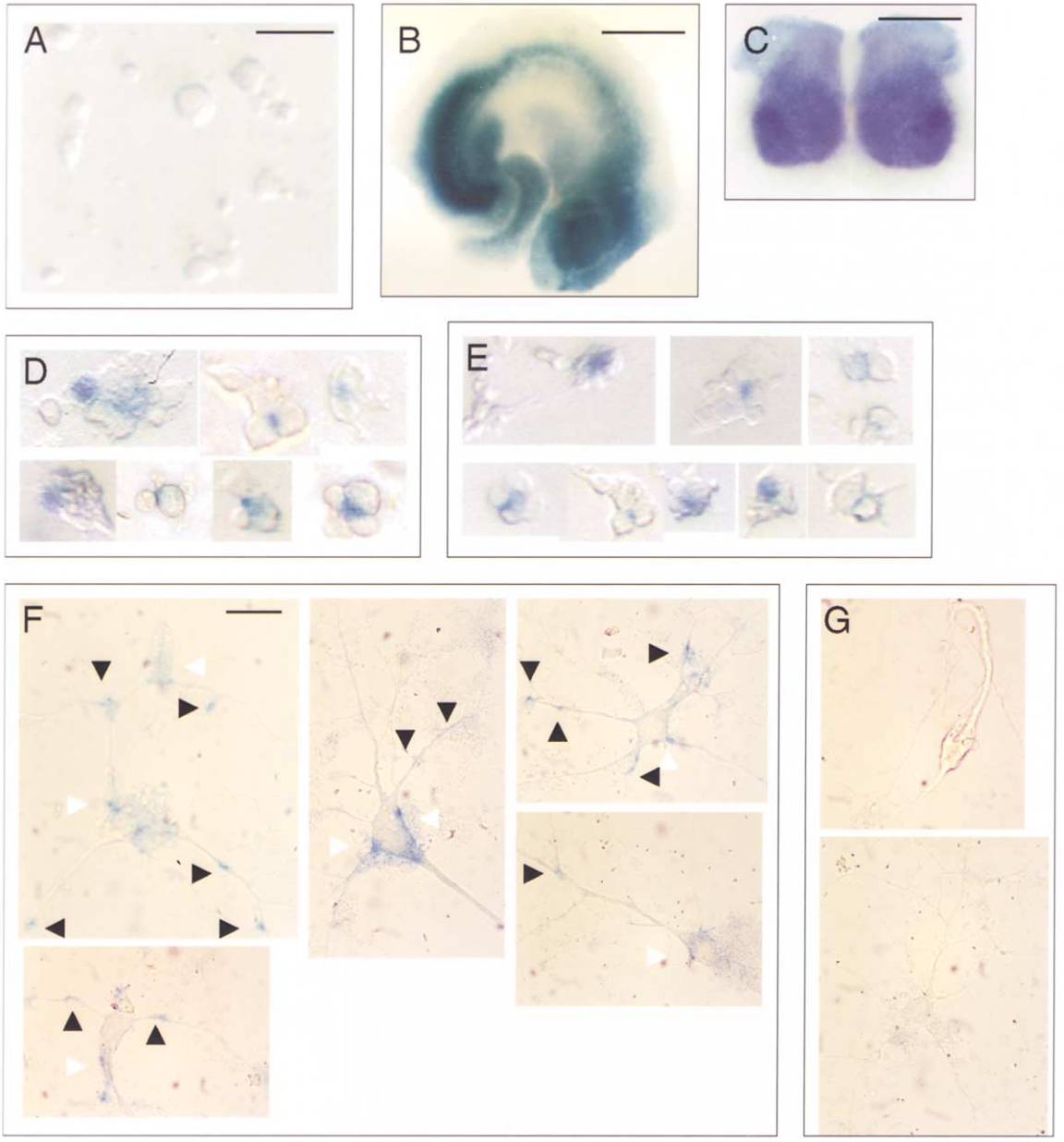

Figure 7. Regulation of EphB2 Expression In Vitro

(A) Hippocampal neurons 20 hr following dissociation at P7 in the absence of inducing stimuli. Scale bar, 30 μm.
(B) Hippocampal explant from P7 *EphB2*$^{N2/+}$ mouse after 7 days in culture.
(C) Spinal cord explant from P7 *EphB2*$^{N2/+}$ mouse after 7 days in culture.
(D) Hippocampal neurons cultured as given in (A) treated with 10 μM kainic acid and 20 μM MK-801 from time of dissociation (20 hr).
(E) Neurons treated with 20 μM NMDA and CNQX.
For (B) and (C) scale bars are 1 mm. For (D) and (E) scale bars are 30 μm.
(F and G) *EphB2*$^{N2/+}$ hippocampal neurons plated at P7 and cultured for 24 days in vitro.
(F) Formation of interpyramidal synapses during this period in culture results in reexpression of EphB2 at sites of synaptic contact in dendrites (closed arrowheads) and cell soma (open arrowheads).
(G) Hippocampal neurons which remain isolated during this period, do not reexpress EphB2.
For (F) and (G) scale bar is 20 μm.

Role of EphB2 in Synaptic Plasticity

LTP is a widely studied form of synaptic plasticity believed to represent a cellular mechanism of learning and memory in the hippocampus (Malenka and Nicoll, 1999; Malinow et al., 2000). Our results demonstrate that for medial perforant path/dentate granule synapses, LTP is strongly attenuated in *EphB2* null mice. As this pathway represents a central input to the core circuitry of the hippocampus, these findings have important implications for subsequent "downstream" neural transmission

within this structure. That *EphB2* null mice exhibit deficiencies in LTP in both the dentate gyrus and CA1 is consistent with observations that these mice are deficient in hippocampal-dependent tasks such as the Morris water maze (Grunwald et al., 2001). Synaptic parameters such as paired-pulse facilitation and input-output responses are unaltered in *EphB2* null mice, suggesting that the defect in LTP reflects alterations in the postsynaptic mechanisms. *EphB2*$^{N2/N2}$ mice exhibited no deficits in LTP, indicating that the kinase domain and carboxy-terminal elements of EphB2 are dispensable with respect to LTP. It is, nonetheless, possible that EphB2 kinase activity has an impact on synaptic function, which is compensated for by other EphB family members or distinct tyrosine kinases in N2/N2 mutants. Previously, intracranial infusion of exogenous Eph/ephrin A5 receptor/ligand bodies have indicated effects on behavior in mice, though the mechanism is unclear (Gao and Phillips, 1999; Gerlai et al., 1999). While the degree of inhibition or activation provided through infusion of these immunoadhesins is difficult to determine, the effects observed likely reflect the results of multiple interactions between EphA/ephrin A family members.

With respect to our LTP data, we observed a more modest reduction in LTP at Schaffer collateral/CA1 synapses compared to perforant path/dentate synapses. This difference may be a function of differences in the relative levels of dendritic EphB2 expression and/or their contribution to NMDARs current at these sites. Alternatively, this difference may reflect the contributions of other EphB receptors and/or ligands in these regions. For example, both EphB2 and EphB1 are strongly expressed in CA1, whereas EphB2 and EphB3 are dominant in dentate granule neurons (Grunwald et al., 2001). It will thus be important to characterize the functional influences of different ephrin/Eph family members at each of these sites.

While the attenuation in LTP observed in *EphB2* null mice could involve several factors, quantitative immunogold labeling for NMDAR1 in dentate granule neurons suggests one possible mechanism. Loss of EphB2 results in a reduction of functional synaptically localized NMDARs. A direct association of EphB2 and NMDAR1 is also supported by biochemical studies of hippocampal neurons in vitro (Dalva et al., 2000; Grunwald et al., 2001). Similar to our LTP data, the association of EphB2 and NMDAR1 in these studies was independent of EphB2 kinase activity. While the precise mechanism by which loss of EphB2 alters the localization of NMDAR1 is unclear in vivo, we suggest that EphB2 may act to stabilize occupancy of NMDARs within the postsynaptic membrane. Alternatively, lack of EphB2 may alter signaling events downstream of EphB2/NMDAR interactions, which ultimately result in the observed changes in NMDAR1 distribution.

Activity-Dependent Regulation of EphB2 at Neural Synapses

The results obtained for hippocampal neurons both in vitro and in vivo demonstrate that in addition to regulating NMDA-dependent synaptic responses, EphB2 can itself be regulated in an activity-dependent manner. Treatment with agents such as kainic acid result in a sustained increase in EphB2 expression within the dentate granule dendrites. Several additional plasticity/injury paradigms failed to elicit increases in EphB2 expression, suggesting that this response exhibits both cell-type and stimulus specificity. That EphB2 may play a functional role in regulating postnatal sprouting following kainic acid treated is suggested from differences in the pattern of mossy fiber sprouting seen in *EphB2* null mice versus controls following treatment.

In dissociated hippocampal neurons, EphB2 expression was rapidly lost in the absence of depolarizing agents such as NMDA and kainic acid. However, EphB2 expression could be maintained continuously for weeks in organotypic explants under similar conditions. Furthermore, pyramidal neurons reexpressed EphB2 at sites of synaptic contact following several weeks in culture. These data suggest that EphB2 expression is regulated by synaptic activity in CNS neurons. The fact that EphB2 regulates both axon guidance during embryonic development and postnatal synaptic function emphasizes the varied and complex roles for this receptor family in regulating cell-cell interactions within the CNS.

Experimental Procedures

Murine Lines/Sample Preparation

For each mutation (m), indicated genotypes were obtained from intercrosses of (+/+) or (+/m) mice with (m/m) animals, maintained on either 129SV/cp or outbred backgrounds. Mice homozygous for the null allele of *EphB2* gene were designated *EphB2*$^{-/-}$, whereas mice homozygous for a targeted mutation of *EphB2* lacking the kinase SAM and PDZ binding sites were designated *EphB2*$^{N2/N2}$, as previously described (Henkemeyer et al., 1996). Mice were anesthetized (sodium pentobarbital, 80 mg/kg), and with the exception of animals for Timm's, Golgi, and β-galactosidase staining, perfused transcardially with 0.1 M phosphate buffered saline (PBS) at pH 7.4, followed by 4% paraformaldehyde in PBS at 4°C. Brains were postfixed and processed as either cryostat (Leitz CM 3050) or paraffin sections (Reichert-Jung 2030 microtome) and analyzed blindly. For DiI labeling, DiI crystals (Molecular Probes) were implanted into the middorsal blade of the dentate using a tungsten needle, left at 37°C for 4 weeks, and then cut into 400 μm coronal sections.

Surgical Procedures

For intrahippocampal delivery of kainic acid and NMDA (0.5 or 1 nmol), 7- to 9-week-old *EphB2* mice were anesthetized, their heads placed in a stereotactic frame, and agents delivered (0.1 μl) via a borosilicate capillary (terminal diameter 50 μm). Cannulae were introduced halfway between the lambda and bregmal sutures, 2 mm lateral to the midline, to a depth of 1.5 mm from the zero plane. Several additional procedures known to induce axonal and/or dendritic remodeling were also performed: (1) monocular deprivation through permanent closure of the right eyelid at P22 with the superior colliculus examined 7 days later (n = 7 animals in three separate experiments) as described (Cao et al., 2000), (2) mystacial vibrissectomy performed on row D whiskers at P0 with mice examined 10 days postinjury (n = 6 animals) as described (Finney and Shatz, 1998) and, (3) cutaneous denervation, performed at P35 with mice examined 2–5 days following injury (n = 4 animals per group) (Doucette and Diamond, 1987).

Histochemistry/Immunohistochemistry (IHC)

Sections were blocked in 5% normal goat serum, 0.2% Tween-20 in PBS for 1 hr at RT followed by incubation in primary antibody 4°C. Primary antisera were as follows: Calbindin D (Sigma) 1:400, calretinin (Chemicon) 1:400, parvalbumin (Sigma) 1:600, mGluR5 (Upstate Biotechnology) 1:1000, Ephrin B1 (C-18 Santa Cruz) 1:1000, and GluR1a (Upstate Biotechnology) 1:3000. Either fluorescent or biotinylated secondary antibodies were used for visualization according to standard protocols. To examine NMDAR1 in Western

analyses, a rabbit polyclonal antibody (Upstate Biotechnology) was used. For EphB2 immunoprecipitations, 1 mg of total protein was incubated with 5 μg/ml EphB2 antiserum for 1 hr at 4°C. Samples were then separated on SDS-PAGE and immunoblotted with appropriate antibodies. For IHC and EM, a mouse monoclonal of NR1 (Pharmingen 54.1) was employed. Anti-EphB2 was used as previously described (Holland et al., 1997). We raised a phosphospecific PAB (435J) to the EphB juxtamembrane region. Purified antisera was used at 1:1000 for immunoprecipitations and Western analyses, and 1:300 for IHC. Staining for β-galactosidase activity was as previously described (Ausubel, 1991).

Timm's/Golgi Staining

Mice were perfused with 50 ml 0.37% sodium sulfide, (pH 7.2) for 5 min, followed by 50 ml 4% paraformaldehyde in PBS. Tissues were processed as previously described (Sloviter, 1982). For Golgi staining, tissues were immersed in 2.6% potassium dichromate, 0.33% osmium tetroxide for 7 days at room temperature in the dark, rinsed briefly in water, and placed in 0.75% silver nitrate for 24 hr at room temperature in the dark. Sections were then processed at 25–50 μm.

Hippocampal Spine Imaging

Hippocampal neurons were imaged using a DeltaVision (Applied Precision) deconvolution microscope (Olympus IX70) in brightfield and fluorescent modes. Neuronal profiles were extracted from serial images collected at 0.2 μm intervals. Numeric counts of dendritic spines on hippocampal CA1 apical dendrites were determined by counting spines in 75 μm segments of apical CA1 dendrites. A minimum of ten dendritic segments were counted in each of four animals per genotype.

EM/Postembedding Immunogold EM

For standard transmission EM, samples were fixed in 2% glutaraldehyde, 2% paraformaldehyde in PBS at 4°C. Samples were impregnated with 1% osmium tetroxide, 2% uranyl acetate, and lead citrate in 0.1 M cacodylate buffer (pH 7.3) (CB) for 1 hr, washed, then dehydrated and embedded in Spurr resin. Seventy nanometer sections were collected onto 200 mesh copper grids and stained with uranyl acetate and Sato's lead citrate. The distal component of the stratum radiatum within the CA1 region and the central third of the molecular layer of dentate gyrus were examined on a Phillips CM 100 electron microscope equipped with a Kodak QRS 2050 digital camera.

For postembedding immunogold IHC of NMDAR1, the dorsal blade of the dentate gyrus and associated molecular layer were subdissected from hippocampi in two pairs of P35 *EphB2*$^{+/-}$ and *EphB2*$^{-/-}$ mice. Samples were fixed in 0.1% glutaraldehyde, 4% paraformaldehyde in CB for 1 hr, dehydrated, then embedded in Lowicryl K4M resin at −20°C. Blocks were polymerized overnight under UV light at −20°C. A series of 70 nm thick sections were then collected at intervals of 350 nm from each tissue block and placed onto numbered Formvar coated 200 mesh nickel grids. Tissue sections were incubated with anti-NMDAR1 MAB (Pharmingen, 1:100) at 4°C for 6 hr, followed by 10 nm gold-conjugated anti-mouse IgG (Amersham; 1:20) for 3 hr at 4°C as described (Milner and Drake, 2001). Samples were then poststained as given above. Fields containing asymetric spiny dendrites within the central third of the dentate molecular layer were examined at 46× and 66,000× magnification. Numbers of gold particles at or within 25 nm of the postsynaptic density (determined by morphological parameters) and along its length were then determined. Density of immunogold labeling per synapse was calculated as a function of its XY area in units of μm^2. For *EphB2*$^{+/-}$ and *EphB2*$^{-/-}$ mice, significant differences were determined by Student's t test following a Kolmogrov-Smirnov test for distribution normality.

Electrophysiology/CA1 Recordings

All chemicals used for electrophysiology were from RBI/Sigma unless otherwise specified. CA1 recordings were as described (Jia et al., 1998). Briefly, field excitatory postsynaptic potentials (fEPSPs) were evoked at a frequency of 0.03 Hz by bipolar tungsten electrodes and recorded with micropipettes filled with ACSF. Responses were amplified with an Axoclamp 2B and analyzed using pCLAMP7 software (Axon Instruments). Field potentials were measured by obtaining slopes of the rising phase between 10% and 90% of peak response and were verified by addition of 5 μM NBQX (RBI/Sigma) at the end of each experiment. Stimulation intensity was adjusted to obtain 25%–30% of maximal fEPSP. Tetani to induce LTP consisted of two trains (10 s apart) at 100 Hz/1s stimulation.

Dentate Granule Recordings

Mice were tested in blind fashion at 4–6 weeks of age. Hippocampal slices were perfused with ACSF consisting of: 124 mM NaCl, 3 mM KCl, 2.5 mM $CaCl_2$, 1.3 mM $MgSO_4$, 1.25 mM NaH_2PO_4, 26 mM $NaHCO_3$, 10 mM D-glucose (pH 7.4, 30°C). In recordings of fEPSPs, 50 μM picrotoxin where indicated was added to block $GABA_A$ receptor-mediated inhibitory synaptic events. Recordings of excitatory postsynaptic currents (EPSCs) were performed in ACSF containing 10 μM bicuculline methiodide and 1 μM CGP-55845 (Tocris) to block $GABA_B$ receptors. Where specified, 100 μM D-AP5 and 2 μM NBQX disodium salt (Tocris) were included to block NMDA and AMPA glutamate receptors, respectively. Application of AP5 together with NBQX did not completely eliminate the EPSC, but the residual currents were not significantly different between genotypes.

Extracellular fEPSPs were obtained using 3 MΩ glass electrodes (containing ASCF lacking Ca^{2+}) and an Axopath 1D (Axon Instruments) amplifier set to filter at 2 kHz and digitized at 10 kHz using pCLAMP6 software. Whole-cell recordings were made using patch pipettes (4–6 MΩ) filled with: 130 mM Cs gluconate, 30 mM HEPES, 11 mM EGTA, 10 mM KCl, 2 mM Mg-ATP, 2 mM QX-314 (lidocaine n-ethyl bromide), 1 mM $CaCl_2$ (pH 7.25, 290 mOsmol/l). Recording pipettes were positioned into the granule cell layer using a 40× water immersion objective on a Nikon E600FN microscope. Input resistance was monitored by a voltage step pulse applied after each EPSC collected. Cells which were not stable were rejected.

The stimulating electrode was positioned in the dorsal blade of the dentate molecular layer to record granule cell dendritic population responses (fEPSPs) or single cell synaptic currents (EPSCs) arising from medial perforant path stimulation. Stimulation intensity was adjusted to yield fEPSPs, which were 30% of the maximal spike free fEPSP size. During tetanic stimulation, pulse duration was increased 3-fold to 0.15 ms. In whole-cell recordings, stimulus intensity was set to 50% of the maximum EPSC obtained at a holding potential of −60 mV. NMDA current was derived pharmacologically by determining the reduction in synaptic current upon addition of D-AP5.

Field responses were recorded every 20s and slope (10%–50%) was normalized to control responses. EPSC recordings were collected every 10 s and measured by peak amplitude. To calculate input-output relationships, stimulus strength was used as a measure of input. Statistical differences were determined by Student's t test.

Cell/Organotypic Culture

Pyramidal and dentate granule neurons (P0-1) were dissociated from micro-dissected hippocampi by trituration and grown on glass coverslips coated with 10 μg/ml ECM (Upstate Biotechnology) for 2 hr at room temperature. For the first 48 hr, hippocampal cultures were grown in 10% fetal calf serum (FCS), 2 mM glutamine, and 10 μM cytosine arabinoside DMEM, then switched into Neurobasal media (GIBCO) supplemented with B27 and 2 mM glutamine for 1–4 weeks. Granule cultures were grown in a medium of 10% FCS, 2 mM glutamine, and 25 mM KCl in DMEM. Kainic acid, NMDA, CNQX, and MK-801 were all from RBI/Sigma and used at concentrations of 10 μM, 20 μM, 20 μM, and 20 μM, respectively.

Stimulation conditions of stable cell lines expressing EphB2 were as described (Holland et al., 1996). For organotypic cultures, P7-35 hippocampi and spinal cords were dissected free of surrounding blood vessels and dura and cut at 300 μm through the central third of the hippocampus or L2 level using a MacIlwain tissue chopper at 4°C. Slices were cultured on Anopore membrane inserts (Nunc), in 10% FCS, 2 mM glutamine, 100 units/ml penicillin-G, 100 μg/ml streptomycin in DMEM for 5–14 days as described (Stoppini et al., 1991). For each experiment, a minimum of six explants per animal were obtained for each of the conditions used and experiments

were repeated a minimum of three times in each of three separate animals.

Acknowledgments

We are indebted to D. Holmyard, M. Mendez, and J. Pittman (Mount Sinai Hospital) for technical assistance and EM support; S. Kulkarni for assistance with deconvolution imaging; D. Stapleton for assistance with protein chemistry; Y. Zhang for assistance with CA1 electrophysiologic recordings; and B. Ju for assistance with hippocampal cultures. In addition, we thank D. Bai and J.M. Wojtowicz for helpful discussion regarding dentate granule recordings. This work was supported by grants from CIHR to J.T.H. and T.P., and by a Howard Hughes Medical Institute International Research Scholar Award, and a CIHR Distinguished Scientist Award to T.P. J.G. was supported by a CNRP (Canadian Neurotrauma Research Program) Fellowship through CIHR.

Received March 9, 2001; revised November 15, 2001.

References

Ausubel, F.M. (1991). Fixation, embedding and sectioning. In Current Protocols in Molecular Biology, F.M. Ausubel, ed. (New York: John Wiley and Sons), pp. 14.1.1–14.1.6.

Bergemann, A.D., Zhang, L., Chiang, M.K., Brambilla, R., Klein, R., and Flanagan, J.G. (1998). Ephrin-B3, a ligand for the receptor EphB3, expressed at the midline of the developing neural tube. Oncogene *16*, 471–480.

Binns, K.L., Taylor, P.P., Sicheri, F., Pawson, T., and Holland, S.J. (2000). Phosphorylation of tyrosine residues in the kinase domain and juxtamembrane region regulates the biological and catalytic activities of Eph receptors. Mol. Cell. Biol. *20*, 4791–4805.

Birgbauer, E., Cowan, C.A., Sretavan, D.W., and Henkemeyer, M. (2000). Kinase independent function of EphB receptors in retinal axon pathfinding to the optic disc from dorsal but not ventral retina. Development *127*, 1231–1241.

Bortolotto, Z.A., Clarke, V.R., Delany, C.M., Parry, M.C., Smolders, I., Vignes, M., Ho, K.H., Miu, P., Brinton, B.T., Fantaske, R., et al. (1999). Kainate receptors are involved in synaptic plasticity. Nature *402*, 297–301.

Brownlee, H., Gao, P.P., Frisen, J., Dreyfus, C., Zhou, R., and Black, I.B. (2000). Multiple ephrins regulate hippocampal neurite outgrowth. J. Comp. Neurol. *425*, 315–322.

Bruckner, K., and Klein, R. (1998). Signaling by Eph receptors and their ephrin ligands. Curr. Opin. Neurobiol. *8*, 375–382.

Buchert, M., Schneider, S., Meskenaite, V., Adams, M.T., Canaani, E., Baechi, T., Moelling, K., and Hovens, C.M. (1999). The junction-associated protein AF-6 interacts and clusters with specific Eph receptor tyrosine kinases at specialized sites of cell-cell contact in the brain. J. Cell Biol. *144*, 361–371.

Cao, Z., Lickey, M.E., Liu, L., Kirk, E., and Gordon, B. (2000). Postnatal development of NR1, NR2A and NR2B immunoreactivity in the visual cortex of the rat. Brain Res. *859*, 26–37.

Carpenter, M.K., Shilling, H., VandenBos, T., Beckmann, M.P., Cerretti, D.P., Kott, J.N., Westrum, L.E., Davison, B.L., and Fletcher, F.A. (1995). Ligands for EPH-related tyrosine kinase receptors are developmentally regulated in the CNS. J. Neurosci. Res. *42*, 199–206.

Chin-Sang, I.D., George, S.E., Ding, M., Moseley, S.L., Lynch, A.S., and Chisholm, A.D. (1999). The ephrin VAB-2/EFN-1 functions in neuronal signaling to regulate epidermal morphogenesis in C. elegans. Cell *99*, 781–790.

Dalva, M.B., Takasu, M.A., Lin, M.Z., Shamah, S.M., Hu, L., Gale, N.W., and Greenberg, M.E. (2000). EphB receptors interact with NMDA receptors and regulate excitatory synapse formation. Cell *103*, 945–956.

Davis, S., Gale, N.W., Aldrich, T.H., Maisonpierre, P.C., Lhotak, V., Pawson, T., Goldfarb, M., and Yancopoulos, G.D. (1994). Ligands for EPH-related receptor tyrosine kinases that require membrane attachment or clustering for activity. Science *266*, 816–819.

Drescher, U. (1997). The Eph family in the patterning of neural development. Curr. Biol. *7*, R799–R807.

Doucette, R., and Diamond, J. (1987). Normal and precocious sprouting of heat nociceptors in the skin of adult rats. J. Comp. Neurol. *261*, 592–603.

Elowe, S., Holland, S.J., Kulkarni, S., and Pawson, T. (2001). Down-regulation of the Ras-mitogen-activated protein kinase pathway by the EphB2 receptor tyrosine kinase is required for ephrin-induced neurite retraction. Mol. Cell. Biol. *21*, 7429–7441.

Finney, E.M., and Shatz, C.J. (1998). Establishment of patterned thalamocortical connections does not require nitric oxide synthase. J. Neurosci. *18*, 8826–8838.

Flanagan, J.G., and Vanderhaeghen, P. (1998). The ephrins and Eph receptors in neural development. Annu. Rev. Neurosci. *21*, 309–345.

Gale, N.W., Holland, S.J., Valenzuela, D.M., Flenniken, A., Pan, L., Ryan, T.E., Henkemeyer, M., Strebhardt, K., Hirai, H., Wilkinson, D.G., et al. (1996). Eph receptors and ligands comprise two major specificity subclasses and are reciprocally compartmentalized during embryogenesis. Neuron *17*, 9–19.

Gao, W., and Phillips, H.S. (1999). Regulation of learning by EphA receptors: a protein targeting study. J. Neurosci. *19*, 9538–9549.

Gao, P.P., Yue, Y., Cerretti, D.P., Dreyfus, C., and Zhou, R. (1999). Ephrin-dependent growth and pruning of hippocampal axons. Proc. Natl. Acad. Sci. USA *96*, 4073–4077.

Gerlai, R., Shinsky, N., Shih, A., Williams, P., Winer, J., Armanini, M., Cairns, B., Winslow, J., Gao, W., and Phillips, H.S. (1999). Regulation of learning by EphA receptors: a protein targeting study. J. Neurosci. *19*, 9538–9549.

Gomperts, S.N., Carroll, R., Malenka, R.C., and Nicoll, R.A. (2000). Distinct roles for ionotropic and metabotropic glutamate receptors in the maturation of excitatory synapses. J. Neurosci. *20*, 2229–2237.

Grunwald, I.C., Korte, M., Wolfer, D., Wilkinson, G.A., Unsicker, K., Lipp, H.-P., Bonhoeffer, T., and Klein, R. (2001). Kinase-independent requirement of EphB2 receptors in hippocampal synaptic plasticity. Neuron *32*, this issue, 1027–1040.

Henkemeyer, M., Orioli, D., Henderson, J.T., Saxton, T.M., Roder, J., Pawson, T., and Klein, R. (1996). Nuk controls pathfinding of commissural axons in the mammalian central nervous system. Cell *86*, 35–46.

Holland, S.J., Gale, N.W., Mbamalu, G., Yancopoulos, G.D., Henkemeyer, M., and Pawson, T. (1996). Bidirectional signalling through the EPH-family receptor Nuk and its transmembrane ligands. Nature *383*, 722–725.

Holland, S.J., Gale, N.W., Gish, G.D., Roth, R.A., Songyang, Z., Cantley, L.C., Henkemeyer, M., Yancopoulos, G.D., and Pawson, T. (1997). Juxtamembrane tyrosine residues couple the Eph family receptor EphB2/Nuk to specific SH2 domain proteins in neuronal cells. EMBO J. *16*, 3877–3888.

Jia, Z., Lu, Y., Henderson, J., Taverna, F., Romano, C., Abramow-Newerly, W., Wojtowicz, J.M., and Roder, J. (1998). Selective abolition of the NMDA component of long-term potentiation in mice lacking mGluR5. Learn. Mem. *5*, 331–343.

Lee, S., Williamson, J., Lothman, E.W., Szele, F.G., Chesselet, M.F., Von Hagen, S., Sapolsky, R.M., Mattson, M.P., and Christakos, S. (1997). Early induction of mRNA for calbindin-D28k and BDNF but not NT-3 in rat hippocampus after kainic acid treatment. Brain Res. Mol. Brain Res. *47*, 183–194.

Lisman, J., Malenka, R.C., Nicoll, R.A., and Malinow, R. (1997). Learning mechanisms: the case for CaM-KII. Science *276*, 2001–2002.

Malenka, R.C., and Nicoll, R.A. (1999). Long-term potentiation—a decade of progress? Science *285*, 1870–1874.

Malinow, R., Mainen, Z.F., and Hayashi, Y. (2000). LTP mechanisms: from silence to four-lane traffic. Curr. Opin. Neurobiol. *10*, 352–357.

Matsunaga, T., Greene, M.I., and Davis, J.G. (2000). Distinct expression patterns of eph receptors and ephrins relate to the structural organization of the adult rat peripheral vestibular system. Eur. J. Neurosci. *12*, 1599–1616.

Meima, L., Kljavin, I.J., Moran, P., Shih, A., Winslow, J.W., and Caras,

I.W. (1997). AL-1-induced growth cone collapse of rat cortical neurons is correlated with REK7 expression and rearrangement of the actin cytoskeleton. Eur. J. Neurosci. *9*, 177–188.

Milner, T.A., and Drake, C.T. (2001). Ultrastructural evidence for presynaptic mu opioid receptor modulation of synaptic plasticity in NMDA-receptor-containing dendrites in the dentate gyrus. Brain Res. Bull. *54*, 131–140.

O'Leary, D.D., and Wilkinson, D.G. (1999). Eph receptors and ephrins in neural development. Curr. Opin. Neurobiol. *9*, 65–73.

Rudge, J.S., Mather, P.E., Pasnikowski, E.M., Cai, N., Corcoran, T., Acheson, A., Anderson, K., Lindsay, R.M., and Wiegand, S.J. (1998). Endogenous BDNF protein is increased in adult rat hippocampus after a kainic acid induced excitotoxic insult but exogenous BDNF is not neuroprotective. Exp. Neurol. *149*, 398–410.

Sans, N., Petralia, R.S., Wang, Y.X., Blahos, J., Hell, J.W., and Wenthold, R.J. (2000). A developmental change in NMDA receptor-associated proteins at hippocampal synapses. J. Neurosci. *20*, 1260–1271.

Shi, S.H., Hayashi, Y., Petralia, R.S., Zaman, S.H., Wenthold, R.J., Svoboda, K., and Malinow, R. (1999). Rapid spine delivery and redistribution of AMPA receptors after synaptic NMDA receptor activation. Science *284*, 1811–1816.

Sloviter, R.S. (1982). A simplified Timm stain procedure compatible with formaldehyde fixation and routine paraffin embedding of rat brain. Brain Res. Bull. *8*, 771–774.

Soderling, T.R., and Derkach, V.A. (2000). Postsynaptic protein phosphorylation and LTP. Trends Neurosci. *23*, 75–80.

Stoppini, L., Buchs, P.A., and Muller, D. (1991). A simple method for organotypic cultures of nervous tissue. J. Neurosci. Methods *37*, 173–182.

Tang, Y.P., Shimizu, E., Dube, G.R., Rampon, C., Kerchner, G.A., Zhuo, M., Liu, G., and Tsien, J.Z. (1999). Genetic enhancement of learning and memory in mice. Nature *401*, 63–69.

Torres, R., Firestein, B.L., Dong, H., Staudinger, J., Olson, E.N., Huganir, R.L., Bredt, D.S., Gale, N.W., and Yancopoulos, G.D. (1998). PDZ proteins bind, cluster, and synaptically colocalize with Eph receptors and their ephrin ligands. Neuron *21*, 1453–1463.

Wang, S., and Wojtowicz, J.M. (1997). Effect of GABA(B) receptors on synaptic interactions in dentate gyrus granule neurons of the rat. Neuroscience *79*, 117–127.

Wang, X., Roy, P.J., Holland, S.J., Zhang, L.W., Culotti, J.G., and Pawson, T. (1999). Multiple ephrins control cell organization in C. elegans using kinase-dependent and -independent functions of the VAB-1 Eph receptor. Mol. Cell *4*, 903–913.

Xu, Q., Mellitzer, G., Robinson, V., and Wilkinson, D.G. (1999). In vivo cell sorting in complementary segmental domains mediated by Eph receptors and ephrins. Nature *399*, 267–271.